Soft Matter

ARTICLE TYPE

Cite this: DOI: 00.0000/xxxxxxxxxx

Supplementary Information: Twist dynamics and buckling instability of ring DNA: the effect of groove asymmetry and anisotropic bending

Yair Augusto Gutiérrez Fosado,[‡a] Fabio Landuzzi,[‡a] and Takahiro Sakaue[*ab]

Contents

[a] *Department of Physics and Mathematics, Aoyama Gakuin University 5-10-1 Fuchinobe, Chuo-ku, Sagamihara-shi, Kanagawa 252-5258, Japan.*
[b] *PRESTO, Japan Science and Technology Agency (JST), 4-1-8 Honcho Kawaguchi, Saitama 332-0012, Japan.*
‡ Joint first authors.

I Statistical mechanics of the TWLC

Here we use standard methods of statistical mechanics to get some important relations for the analysis presented in the main text. To this end, we first write the discretized free energy functional ($E=\int_0^L \varepsilon_0(\mathbf{\Omega})ds$) at the base-pair level, with ε_0 given by Eq. (2):

$$\begin{aligned} E &= \frac{a}{2}\sum_{n=1}^{N}[A_1\Omega_1^2(n)+A_2\Omega_2^2(n)+C\Omega_3^2(n) \\ &\quad +2GC\Omega_2(n)\Omega_3(n)] \\ &= \frac{a}{2}\sum_{n=1}^{N}[A_1\Omega_1^2(n)+A_2[\Omega_2(n)+\frac{G}{A_2}\Omega_3(n)]^2 \\ &\quad +\tilde{C}\Omega_3^2(n)], \end{aligned} \tag{S1}$$

where $\Omega_i(n)$ with $i=1,2,3$, represents the local deformation i at position n. Therefore, the probability that the system is in a state with energy E is given by:

$$P=\frac{e^{-\beta E}}{Z}, \tag{S2}$$

where Z is the partition function:

$$Z=\int \mathscr{D}[\mathbf{\Omega}]e^{-\beta E}, \tag{S3}$$

and $\mathscr{D}[\mathbf{\Omega}]$ is the infinitesimal "volume" element in the $\mathbf{\Omega}$ space.

As described in the main text, the probability-weight $P(\{\Omega_i\})$ of finding the system with a characteristic Ω_i, is obtained by integrating out Eq. S2 along the two other local deformations. Then, for Ω_3 we get the following relation:

$$\begin{aligned} P(\{\Omega_3\}) &= \frac{1}{Z}\prod_{n=1}^{N}\iint e^{-\frac{\beta a}{2}[A_1\Omega_1^2+A_2(\Omega_2+\frac{G}{A_2}\Omega_3)^2+\tilde{C}\Omega_3^2]}d\Omega_1 d\Omega_2 \\ &= \frac{1}{Z}\left(\frac{4\pi^2}{\beta^2 a^2 A_1 A_2}\right)^{N/2}\prod_{n=1}^{N}e^{-\frac{\beta a}{2}\tilde{C}\Omega_3^2}. \end{aligned} \tag{S4}$$

The analogous calculation for Ω_2 gives:

$$P(\{\Omega_2\})=\frac{1}{Z}\left(\frac{4\pi^2}{\beta^2 a^2 A_1 C}\right)^{N/2}\prod_{n=1}^{N}e^{-\frac{\beta a}{2}\tilde{A}_2\Omega_2^2}. \tag{S5}$$

Therefore, the rescaled constants $\tilde{C}=C\left(1-\frac{G^2}{A_2 C}\right)$ and $\tilde{A}_2=A_2\left(1-\frac{G^2}{A_2 C}\right)$ that appear in the exponential functions above, imply the softening of the twisting and bending response, respectively.

One additional observation is that the average $\langle\mathscr{O}\rangle_{\Omega_3}$ of any observable $\mathscr{O}$ at a constant value of Ω_3 is found through the following equation:

$$\langle\mathscr{O}\rangle_{\Omega_3}=\frac{1}{Z}\int\mathscr{D}[\Omega_1,\Omega_2]\mathscr{O}e^{-\beta E}. \tag{S6}$$

Therefore, the averages $\langle\Omega_1\rangle_{\Omega_3}$ and $\langle\Omega_2+\frac{G}{A_2}\Omega_3\rangle_{\Omega_3}$ are found to be zero. This key result implies that the internal torques of the molecule, M_1 and M_2, are also zero.

Finally, it is worth noting that the calculations presented here can be generalized to the ones of a ring molecule by replacing the energy of the system (Eq. (2)) by the appropriate one (Eq. (3)), and rewriting it in terms of the deviations $\delta\Omega_i(s)=\Omega_i(s)-\Omega_i^0(s)$ of the deformations $\Omega_i(s)$, in a similar way to what is done at the beginning of the next section. The outcome of this approach is that we obtain similar equations to the ones displayed here but with Ω_i replaced by $\delta\Omega_i$: $\langle\delta\Omega_1\rangle_{\delta\Omega_3}=0$ and $\langle\delta\Omega_2+\frac{G}{A_2}\delta\Omega_3\rangle_{\delta\Omega_3}=0$.

II Internal torque components

The energy density for a torsionally constraint ring is given by Eq. (3), where the term with Lagrange multiplier μ enforces the bending ($\mathbf{\Omega}_b=\mathbf{\Omega}_1+\mathbf{\Omega}_2$) to take place along the unitary vector $\hat{\boldsymbol{x}}=\sin(\chi s)\hat{\boldsymbol{e}}_1+\cos(\chi s)\hat{\boldsymbol{e}}_2$ pointing in the direction perpendicular to the plane spanned by the molecule. The term with the second multiplier λ accounts for the presence of twist excess $\Delta\chi=\chi-\chi_0$.

The components of the internal torque are found by computing the derivative of the energy density with respect to the elastic strain: $M_i=\frac{\delta\varepsilon}{\delta\Omega_i}$. Here we write the results in terms of the deviations $\delta\Omega_i(s)=\Omega_i(s)-\Omega_i^0(s)$ of the deformations $\Omega_i(s)$ with respect the minimum energy state $\Omega_i^0(s)$ (given in Eq. (4)).

Using $\delta\Omega_i(s)$, the energy density is rewritten as:

$$\begin{aligned} \varepsilon(s) &= \frac{A_1}{2}\delta\Omega_1^2+\frac{A_2}{2}\delta\Omega_2^2+\frac{C}{2}\delta\Omega_3^2+G\delta\Omega_2\delta\Omega_3 \\ &\quad +\epsilon_G(s), \end{aligned} \tag{S7}$$

where $\epsilon_G(s)\equiv\varepsilon(\Omega_1^0,\Omega_2^0,\Omega_3^0)$ represents the ground state energy density, thus, independent of $\delta\Omega_i$. Note that the ground energy density is

$$\begin{aligned} \epsilon_G(s) &= -\frac{\mu^2}{2A_1}\sin^2(\chi s)-\frac{\mu^2}{2\tilde{A}_2}\cos^2(\chi s) \\ &\quad -\frac{\lambda^2}{2\tilde{C}}+\mu\lambda\frac{G}{\tilde{A}_2 C}\cos\chi s, \end{aligned} \tag{S8}$$

and its contour integral

$$\int_G^L \epsilon_G(s)\,ds=-\left(\frac{k_B T}{2}\frac{l_b}{R_0^2}+\frac{\tilde{C}}{2}\Delta\chi^2\right)L, \tag{S9}$$

is formally identical to the energy of torsionally stressed ring (with radius of curvature R_0 and the average excess twist density $\Delta\chi$) made from isotropic TWLC with the bending and twisting moduli $\tilde{A}$ and $\tilde{C}$, respectively[1]. Since $\partial\varepsilon/\partial\Omega_i=\partial\varepsilon/\partial(\delta\Omega_i)$, we

find

$$M_1 = A_1\delta\Omega_1, \tag{S10}$$

$$M_2 = A_2\delta\Omega_2 + G\delta\Omega_3, \tag{S11}$$

$$M_3 = C\delta\Omega_3 + G\delta\Omega_2. \tag{S12}$$

The tangential component of the derivative of the internal torque ($\mathbf{M} = M_1\hat{\boldsymbol{e}}_1 + M_2\hat{\boldsymbol{e}}_2 + M_3\hat{\boldsymbol{e}}_3$) with respect s is obtained by using the relation in Eq. (1) and by noticing that the only non-vanishing terms are the following:

$$\begin{aligned}\frac{d\mathbf{M}}{ds}\cdot\hat{\boldsymbol{e}}_3 =& \left[M_1\frac{d\hat{\boldsymbol{e}}_1}{ds} + M_2\frac{d\hat{\boldsymbol{e}}_2}{ds}\right]\cdot\hat{\boldsymbol{e}}_3 + \frac{dM_3}{ds}\\ =& M_2\Omega_1 - M_1\Omega_2 + \frac{dM_3}{ds}\\ =& A_2\Omega_1\delta\Omega_2 - A_1\Omega_2\delta\Omega_1 + G\Omega_1\delta\Omega_3 + \\ & \frac{d}{ds}(C\delta\Omega_3 + G\delta\Omega_2).\end{aligned} \tag{S13}$$

III Compatibility relation

The derivative of the local reference frame with respect to the intrinsic length, s, and time, t, are expressed by the relation:

$$\frac{\partial\hat{\boldsymbol{e}}_\alpha}{\partial s} = \boldsymbol{\Omega}_{\mathrm{T}}(s,t)\times\hat{\boldsymbol{e}}_\alpha(s,t), \tag{S14}$$

$$\frac{\partial\hat{\boldsymbol{e}}_\alpha}{\partial t} = \boldsymbol{\omega}(s,t)\times\hat{\boldsymbol{e}}_\alpha(s,t). \tag{S15}$$

Compared to Eq. (1) we have simplified notation in Eq. (S14) by defining a total strain vector $\boldsymbol{\Omega}_{\mathrm{T}}(s) = \boldsymbol{\Omega}(s) + \chi_0(s)\hat{\boldsymbol{e}}_3(s)$, where χ_0 is the intrinsic twist rate. Now if we consider the combined action of space and time on the reference frame, since s and t are independent variables, they must commute and we could write the equation:

$$\begin{aligned}0 =& \frac{\partial}{\partial t}\frac{\partial\hat{\boldsymbol{e}}_\alpha}{\partial s} - \frac{\partial}{\partial s}\frac{\partial\hat{\boldsymbol{e}}_\alpha}{\partial t}\\ =& \frac{\partial}{\partial t}[\boldsymbol{\Omega}_{\mathrm{T}}\times\hat{\boldsymbol{e}}_\alpha] - \frac{\partial}{\partial s}[\boldsymbol{\omega}\times\hat{\boldsymbol{e}}_\alpha]\\ =& \frac{\partial\boldsymbol{\Omega}_{\mathrm{T}}}{\partial t}\times\hat{\boldsymbol{e}}_\alpha + \boldsymbol{\Omega}_{\mathrm{T}}\times\frac{\partial\hat{\boldsymbol{e}}_\alpha}{\partial t} - \frac{\partial\boldsymbol{\omega}}{\partial s}\times\hat{\boldsymbol{e}}_\alpha - \boldsymbol{\omega}\times\frac{\partial\hat{\boldsymbol{e}}_\alpha}{\partial s}\\ =& \left[\frac{\partial\boldsymbol{\Omega}_{\mathrm{T}}}{\partial t} - \frac{\partial\boldsymbol{\omega}}{\partial s}\right]\times\hat{\boldsymbol{e}}_\alpha + \boldsymbol{\Omega}_{\mathrm{T}}\times\frac{\partial\hat{\boldsymbol{e}}_\alpha}{\partial t} - \boldsymbol{\omega}\times\frac{\partial\hat{\boldsymbol{e}}_\alpha}{\partial s}\\ =& \left[\frac{\partial\boldsymbol{\Omega}_{\mathrm{T}}}{\partial t} - \frac{\partial\boldsymbol{\omega}}{\partial s}\right]\times\hat{\boldsymbol{e}}_\alpha + \boldsymbol{\Omega}_{\mathrm{T}}\times[\boldsymbol{\omega}\times\hat{\boldsymbol{e}}_\alpha]\\ & - \boldsymbol{\omega}\times[\boldsymbol{\Omega}_{\mathrm{T}}\times\hat{\boldsymbol{e}}_\alpha].\end{aligned} \tag{S16}$$

Using the property of the cross product $a\times(b\times c) = b(a\cdot c) - c(a\cdot b)$ on the last two terms we get

$$\begin{aligned}\left[\frac{\partial\boldsymbol{\omega}}{\partial s} - \frac{\partial\boldsymbol{\Omega}_{\mathrm{T}}}{\partial t}\right]\times\hat{\boldsymbol{e}}_\alpha =& \boldsymbol{\omega}[\boldsymbol{\Omega}_{\mathrm{T}}\cdot\hat{\boldsymbol{e}}_\alpha] - \hat{\boldsymbol{e}}_\alpha[\boldsymbol{\Omega}_{\mathrm{T}}\cdot\boldsymbol{\omega}] - \boldsymbol{\Omega}_{\mathrm{T}}[\boldsymbol{\omega}\cdot\hat{\boldsymbol{e}}_\alpha]\\ & + \hat{\boldsymbol{e}}_\alpha[\boldsymbol{\omega}\cdot\boldsymbol{\Omega}_{\mathrm{T}}]\\ =& \boldsymbol{\omega}[\boldsymbol{\Omega}_{\mathrm{T}}\cdot\hat{\boldsymbol{e}}_\alpha] - \boldsymbol{\Omega}_{\mathrm{T}}[\boldsymbol{\omega}\cdot\hat{\boldsymbol{e}}_\alpha(s,t)]\\ =& \boldsymbol{\omega}[\hat{\boldsymbol{e}}_\alpha\cdot\boldsymbol{\Omega}_{\mathrm{T}}] - \boldsymbol{\Omega}_{\mathrm{T}}[\hat{\boldsymbol{e}}_\alpha\cdot\boldsymbol{\omega}(s,t)]\\ =& \hat{\boldsymbol{e}}_\alpha\times[\boldsymbol{\omega}\times\boldsymbol{\Omega}_{\mathrm{T}}]\\ =& -[\boldsymbol{\omega}\times\boldsymbol{\Omega}_{\mathrm{T}}]\times\hat{\boldsymbol{e}}_\alpha.\end{aligned}$$

As the above relation holds for any component α, we get the compatibility relation:

$$\frac{\partial\boldsymbol{\Omega}_{\mathrm{T}}}{\partial t} - \frac{\partial\boldsymbol{\omega}}{\partial s} - \boldsymbol{\omega}\times\boldsymbol{\Omega}_{\mathrm{T}} = 0. \tag{S17}$$

Using the fact that the intrinsic twist rate χ_0 is independent of time, one can rewrite the above equation into the following form:

$$\frac{\partial\boldsymbol{\Omega}(s,t)}{\partial t} = \frac{\partial\boldsymbol{\omega}(s,t)}{\partial s} + \boldsymbol{\omega}(s,t)\times\boldsymbol{\Omega}(s,t). \tag{S18}$$

The dependence on the reference frame could be worked out

$$\begin{aligned}\frac{\partial\Omega_\alpha}{\partial t}\hat{\boldsymbol{e}}_\alpha + \Omega_\alpha\frac{\partial\hat{\boldsymbol{e}}_\alpha}{\partial t} &= \frac{\partial\omega_\alpha}{\partial s}\hat{\boldsymbol{e}}_\alpha + \omega_\alpha\frac{\partial\hat{\boldsymbol{e}}_\alpha}{\partial s} + \boldsymbol{\omega}\times\boldsymbol{\Omega}\\ \frac{\partial\Omega_\alpha}{\partial t}\hat{\boldsymbol{e}}_\alpha + \boldsymbol{\omega}\times\boldsymbol{\Omega} &= \frac{\partial\omega_\alpha}{\partial s}\hat{\boldsymbol{e}}_\alpha + \boldsymbol{\Omega}_{\mathrm{T}}\times\boldsymbol{\omega} + \boldsymbol{\omega}\times\boldsymbol{\Omega}\\ \frac{\partial\Omega_\alpha}{\partial t}\hat{\boldsymbol{e}}_\alpha &= \frac{\partial\omega_\alpha}{\partial s}\hat{\boldsymbol{e}}_\alpha + \boldsymbol{\Omega}_{\mathrm{T}}\times\boldsymbol{\omega}\end{aligned}$$

From this equation it is immediate to show the projection along the $\hat{\boldsymbol{e}}_3$ axis:

$$\frac{\partial\Omega_3}{\partial t} = \frac{\partial\omega_3}{\partial s} + \Omega_1\omega_2 - \Omega_2\omega_1 \tag{S19}$$

The angular velocity ω_3 on the left could be obtained from the torque balance equation, while the last term is related to the writhe and could be rewritten as $\Omega_1\omega_2 - \Omega_2\omega_1 = (\hat{\boldsymbol{e}}_3\times\partial_s\hat{\boldsymbol{e}}_3)\cdot\partial_t\hat{\boldsymbol{e}}_3$

IV DNA supercoiling

For closed DNA molecules the number of times that the two strands winds around each other (the linking number Lk) is a topological invariant. Further more, under this circumstances the well known White-Fuller-Calugarenau theorem[3] must be satisfied. This theorem states that the linking number can be expressed as the sum of two quantities: twist (Tw) and writhe (Wr). The former represents the extent of rotation of the two strands around the DNA axis and the latter represents the number of self-crossings of the DNA centerline.

The DNA double helix has a preferred configuration where the two strands wrap around each other approximately once every 10.5 base pairs. In this configuration the linking number has a characteristic value $\mathrm{Lk}_0 \simeq N/10.5$. A DNA molecule whose link-

Elastic parameter	From reference [2]		Simulations at 15 K		Simulations at 300 K	
	oxDNA1	oxDNA2	oxDNA1	oxDNA2	oxDNA1	oxDNA2
$\beta_{300} A_1$	51	51	53	53	52	52
$\beta_{300} A_2$	30	37	30	36	30	36
$\beta_{300} C$	77	74	98	95	81	78
$\beta_{300} G$	0	22	0	24	0	22
$\beta_{300} \tilde{C}$	77	66	98	79	81	65
$\beta_{300} \tilde{A}_2$	30	31	30	30	30	30
l_b	38	38	38	38	38	38

Table S1 Elastic parameters reported in nm and computed using Eq. S22 for: simulations reported on reference [2] (with $N = 150$ bp, $T = 300$ K and $[Na^+] = 0.5M$) and simulations performed here (with $N = 312$ bp and $[Na^+] = 1M$) at two different temperatures: $T = 15$ K and $T = 300$ K. Note that $\beta_{300} = 1/(k_B\, 300K)$.

ing number differs from the one in the relaxed state is said to be supercoiled. Therefore, the superhelical density:

$$\sigma = \frac{\Delta \mathrm{Lk}}{\mathrm{Lk}_0} = \frac{\mathrm{Lk} - \mathrm{Lk}_0}{\mathrm{Lk}_0}, \tag{S20}$$

is a quantitative measure of DNA supercoiling. In this manuscript we work mainly with molecules that are 312 bp long. Therefore we expect $\mathrm{Lk}_0 = 30$. While the undertwisted molecule is initialized with $\mathrm{Lk} = 29$, the overtwisted molecule has $\mathrm{Lk} = 31$. Therefore we expect for these cases a small level of supercoiling $|\sigma| = 0.033$.

V Elastic parameters

The elastic parameters of the oxDNA model have been thoroughly characterized in reference [4] for linear DNA molecules, 150 bp long at a temperature of 300 K and using a salt concentration of $[Na^+] = 0.5M$. There, the authors found that the local stiffness parameters associated to the deformation at the single base-pair level ($m = 1$ data in supplementary Fig. S3 of [4] and also reported in SM of [2]) are: for oxDNA1 $\beta A_1 = 51$ nm, $\beta A_2 = 30$ nm, $\beta C = 77$ nm and $G = 0$ while for oxDNA2 $\beta A_1 = 51$ nm, $\beta A_2 = 37$ nm, $\beta C = 74$ nm and $\beta G = 22$ nm. It should be stressed here that the β dependence of these parameters (that does not appear explicitly in the cited references) comes from our choice of notation when defining the free energy of the system (Eq. (2)). By using these values, the rescaled persistence length ($l_{bI} = 37.8$ nm, $l_{bII} = 38.14$ nm), bending rigidity about $\hat{\boldsymbol{e}}_2$ ($\beta \tilde{A}_{2I} = 30$ nm, $\beta \tilde{A}_{2II} = 30.46$ nm) and torsional stiffness ($\beta \tilde{C}_I = 77$ nm and $\beta \tilde{C}_{II} \simeq 61$ nm) can be found for both models: oxDNA1 (I) and oxDNA2 (II). The ratio $\tilde{C}_{II}/\tilde{C}_I = 0.791$ is used in the main text when comparing the diffusion coefficient of both models. We will also use $\tilde{C}_I/\tilde{A}_I = 2.04$ and $\tilde{C}_{II}/\tilde{A}_{II} = 1.6$ in order to compute the bending modes (Eq. (S30)).

Temperature dependence

Here we investigate the effect of the temperature on the value of the elastic parameters for the oxDNA models. To this end, MD simulations were performed on 312 linear DNA molecules at a salt concentration of $[Na^+] = 1M$ and using only GC pairs in the sequence. Each simulation was run for 5×10^7 timesteps while the trajectories were recorded every 10^5 timesteps. A total of eleven independent replicas were used for: oxDNA1 (15 K), oxDNA1 (300 K), oxDNA2 (15 K) and oxDNA2 (300 K). For each case, we found the local deformations (see section VII for details) and we computed the following correlation matrix (see reference [4]):

$$\Xi_{\mu\nu}(m) \equiv \left\langle \left[\sum_{k=n}^{n+m-1} \Omega_\mu(k) \right] \left[\sum_{l=n}^{n+m-1} \Omega_\nu(l) \right] \right\rangle \tag{S21}$$

Finally, the m-step stiffness matrix is defined as:

$$\mathbf{M}(m) \equiv \frac{m}{a} [\boldsymbol{\Xi}(m)]^{-1}, \tag{S22}$$

from which the elastic constants were computed. Results are shown in Fig. S1. Continuous lines represent the values obtained from the simulations at $T = 300$ K, while dashed lines represent values obtained at $T = 15$ K (and rescaled by the factor $15/300 = 0.05$). We observe that for the same oxDNA model, the elastic parameters A_1, A_2 and G do not change with the temperature (apart from the re-scaling constant 0.05). The torsional stiffness C on the other hand, is slightly larger for the case $T = 15$ K.

The local stiffness parameters associated to the deformation at the single base-pair level ($m = 1$) are summarized in Table S1 for three different cases. These results suggest that when decreasing the temperature in our simulations from 300 K to 15 K, C is the only elastic constant that is significantly affected. However, this change is such that the ratio $\tilde{C}_{II}/\tilde{C}_I$ is essentially the same for the three cases: 0.79 (for the elastic constants in [2,4]) and 0.8 in

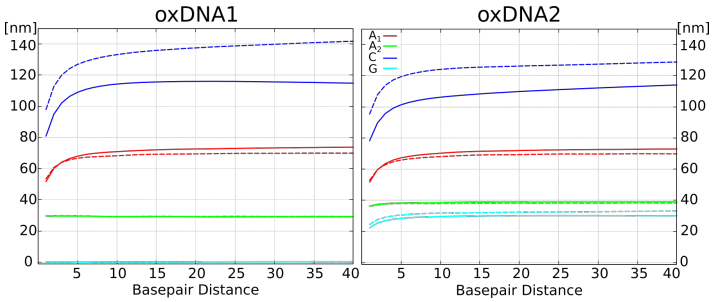

Fig. S1 Elastic parameters obtained from Eq. (S22), as a function of the base-pair distance m.(**A**)-(**B**) Show results for oxDNA1 and oxDNA2, respectively. Continuous and dashed lines represent results from simulations at $T = 300$ K and $T = 15$ K,respectively.

the other two cases. Therefore, all these results are in good agreement with the theory described in this manuscript, which predicts $\tilde{D}_{II}/\tilde{D}_I = \tilde{C}_{II}/\tilde{C}_I \sim 0.8$.

Sequence dependence of the renormalized twist modulus

The values of the elastic parameters for different DNA sequences simulated with oxDNA models, are reported in Fig.S4 and Table S2 of reference[4]. By entering those values in the equation that defines the renormalized twist modulus ($\tilde{C} = C\left(1 - \frac{G^2}{A_2 C}\right)$), we find the values of $\tilde{C}_I$ and $\tilde{C}_{II}$ reported in Table S2 for the two oxDNA models. We observe that for both models, the largest twist modulus is the one of the poly CG sequence. On the other hand, the poly AT sequence have the smallest twist modulus. This might be related to the fact that decreasing the CG content tends to soften the elastic response of the DNA. When comparing the values of $\tilde{C}$ for the same oxDNA model, we found that there is a change of approximately 12.5% for the two sequences mentioned above. Remarkably, the ratio $\tilde{C}_{II}/\tilde{C}_I$ does not exhibit strong deviations for the sequences studied here.

Sequence	$\tilde{C}_I$	$\tilde{C}_{II}$	$\tilde{C}_{II}/\tilde{C}_I$
Avg sequence	116	82	0.70
poly AT	108	76	0.70
poly CG	123	87	0.70
poly AC	115	82	0.71
poly AG	115	80	0.70
A-rich	111	80	0.72
C-rich	118	82	0.69

Table S2 Renormalized twist modulus $\tilde{C}_I$ (for oxDNA1) and $\tilde{C}_{II}$ (for oxDNA2), reported in nm and computed with the values of the elastic parameters found in reference[4], for the sequence shown in the first column. The last column shows the ration $\tilde{C}_{II}/\tilde{C}_I$.

VI Details of simulations

The Langevin integration of the system was carried out in the most recent implementation[5] of the oxDNA model into the LAMMPS[6] (Large Scale Molecular Massively Parallel Simulator) engine. Briefly, this model describes DNA at the single nucleotide level by means of a rigid body with additive-pairwise interaction sites. The potentials involved in the interactions accurately represent: the hydrogen bonding between complementary bases, the connectivity of the sugar-phosphate backbone, the excluded volume between nucleotides and also the stacking, coaxial-stacking and cross-stacking forces. Hence, if U represents the total potential field experienced by the nucleotides and $\mathbf{r}$ their position, then the system obeys the Langevin-equation:

$$m\frac{d^2\mathbf{r}}{dt^2} = -\xi\frac{d\mathbf{r}}{dt} - \nabla U + \sqrt{2k_BT\xi}\Lambda(t), \qquad \text{(S23)}$$

where m is the mass of the nucleotide, ξ is the friction and $\Lambda(t)$ is the white noise term with zero mean which satisfies $\langle\Lambda_\alpha(t)\Lambda_\beta(s)\rangle = \delta_{\alpha\beta}\delta(s-t)$ along each Cartesian coordinate represented by the Greek letters. The form of the last term in Eq. (S23) ensures that the equipartition theorem is satisfied.

Mapping of simulation units – The relation between one simulation unit (SU) in the oxDNA code and the international system (SI) units, is the following: mass ($M = 100\text{AMU} = 1.66\times10^{-25}$ kg), temperature ($T = 3000$ K), length ($L_s = 8.518\times10^{-10}$ m), energy ($\varepsilon_s = k_BT = 4.142\times10^{-20}$ J) and force ($F = \varepsilon_s/L_s = 4.863\times10^{-11}$ N). The simulation time $\tau_{LJ} = L_s\sqrt{M/\varepsilon_s} = 1.7$ ps, comes naturally from the above quantities and it is employed to define a constant integration timestep $\Delta t = 0.001\tau_{LJ}$ of the Langevin equation (S23). In principle, τ_{LJ} could be used to compare results with experiments. However, since the hydrodynamic effects are neglected in the Langevin formalism, one needs to be cautious in interpreting time units in this type of coarse-grained simulations.

It is also important to recognize that there are two further time scales in the system with an intuitive physical meaning. One is the inertial time $\tau_{in} = m/\xi$, which gives the characteristic time after which the velocity of a bead becomes uncorrelated. The second is the Brownian time $\tau_{Br} = (2r_0)^2/D$, which gives the order of magnitude of the time it takes for a bead to diffuse across its own diameter ($2r_0$). Here D is the translational diffusion constant for a bead, given through the Einstein relation by $D = k_BT/\xi$. In the approximation in which a nucleotide diffuses like a sphere with radius $r_0 = 1$ nm, we can use Stokes' law $\xi = 6\pi\eta r_0$, where η is the viscosity of the fluid. Therefore, setting the values of D (or similarly the value of η) and m, will resolve the two additional timescales. For example, if we consider that the mass of individual nucleotides is ($m = 315.75\text{AMU} = 5.24\times10{-}25$ kg) and they are immerse in water ($\eta = 1.1\times10^{-3}\text{kgm}^{-1}\text{s}^{-1}$), we find $\tau_{in} = 5.05\times10^{-14}\text{s} \simeq 0.03\tau_{LJ}$ and $\tau_{Br} = 2.5\times10^{-10}\text{s} \simeq 150\tau_{LJ}$; with the timescales separated by several orders of magnitude ($\tau_{in} \ll \tau_{LJ} \ll \tau_{Br}$).

As pointed out in references[7,8], due to the limitations in our calculations when neglecting the hydrodynamic effects, the diffusion coefficient (and then also τ_{in}) could be seriously underestimated. Therefore, we need to bear in mind the timescales of interest in our system, before choosing the magnitude of D. For instance, in order to investigate the fast process of twist diffusion (not to be confused with D), which occurs at short time-scales, we use the default value of the inertial time ($\tau_{in} = 0.03$) given in the original parametrization of the model. On the other hand, the supercoiling of the molecule occurs at a much larger time-scale. Setting such a low inertial time would lead to prohibitively slow writhing dynamics and unfeasibly long simulations. Instead we chose larger diffusion coefficients (see section IX for details) such that $\tau_{in} \leq \tau_{LJ} \leq \tau_{Br}$. This assumption means that bodies have more inertia than in reality and that processes which occur on time-scales below the Brownian time are not resolved accurately, however this is of no practical consequence for our purpose.

It should be emphasized here that this artificial change of the diffusion, makes difficult to map the simulation time onto real units. We then prefer to report our results in units of τ_{LJ} and to focus on the comparison of times between similar processes.

Additional features of the MD simulations – In the simulations, a ring molecule of $N = 312$ bp was initialized with a deficit of twist. However, when not set properly, undertwisting

encourages the local melting of the base-pairs, creating small regions where the dsDNA splits into its two single-strand components and therefore where the local twist can not be defined. To avoid this, we set appropriate physiological and geometrical conditions: (i) we used a High salt concentration of $[Na^+] = 1M$. The Debye Huckel potential implemented in the oxDNA model allows to effectively modulate the electrostatic interaction of the nucleotides by setting the salt concentration of the system. A high value corresponds to the screening of the negatively charged phosphates of DNA, which prevents melting. (ii) We simulated poly-C molecules. Because G-C pairs form three hydrogen bonds, while A-T pairs form only two, the hydrogen bonding energy of the former is larger than the latter in the oxDNA model. Therefore we use a DNA sequence made of only G-C pairs (homopolymer). As discuss in the main text, this also ensures that the elastic parameters (G, C, A_1 and A_2) do not depend on the position (s) along the dsDNA. (iii) We set a low level of supercoiling in the initial configuration. Under no torsional stress the total twist of a 312 bp ring molecule is $\mathrm{Tw}_0 = 30$. At $t = 0$ we start from a conformation with $\mathrm{Tw} = 29$ and $\mathrm{Wr} = 0$. This corresponds to a supercoiling $\sigma = \Delta\mathrm{Tw}/\mathrm{Tw}_0 = -0.033$. This deficit was split among half of the ring so the local twist deficiency is small enough to avoid melting. This choice also discourages the formation of strong deviation from the planar ring configuration. (iv) Simulations were run at a low temperature ($T = 15$ K). Besides favoring the hybridization of the two single strands, such a low temperature also allows to study the twist Diffusion in the absence of thermal fluctuations and in consequence less simulations have to be performed to get a good statistics. In addition, as discussed in reference [1]; in short, constrained and highly bent DNA, thermal fluctuations are not the main factor influencing the shape of the molecule. Finally, we also analyzed the analogous scenario for over-twisted molecules of DNA using the same conditions of the system and opposite supercoiling level ($\sigma = 0.033$). As mentioned in the main text, when measuring local twist diffusion (see Fig. **3**), the system was confined in between two parallel planes to avoid the writhe formation. On the other hand, when we study the evolution of total twist (see Fig. **5**), the planes were removed.

VII Computation of local Twist

In order to obtain the local deformations (Ω_i) from our simulations, we consider DNA as a discrete inextensible elastic rod. As described in reference [4], this discretization allows to define a local reference frame $\{\hat{\boldsymbol{e}}_1(n), \hat{\boldsymbol{e}}_2(n), \hat{\boldsymbol{e}}_3(n)\}$ at base-pair n along the rod, using the following method. In the oxDNA model the orientation of individual nucleotides is given by two vectors: the normal to the plane of the base ($\hat{\boldsymbol{n}}$), which follows the $5'-3'$ direction of single strands; and the unitary vector ($\hat{\boldsymbol{b}}$), pointing from the backbone site to the base site. The intrinsic nucleotide triad is completed with a third axis defined by $\hat{\boldsymbol{n}} \times \hat{\boldsymbol{b}}$. When the DNA molecule is fully hybridized, both, the vectors $\hat{\boldsymbol{n}}_1$, $\hat{\boldsymbol{n}}_2$ that are part of the triads from two complementary nucleotides in a base-pair and their respective center of mass ($\hat{\boldsymbol{r}}_1$, $\hat{\boldsymbol{r}}_2$), become a natural choice to define the base-pair local reference frame. The tangent to the centerline of the dsDNA is $\hat{\boldsymbol{e}}_3 = (\hat{\boldsymbol{n}}_1 - \hat{\boldsymbol{n}}_2)/|\hat{\boldsymbol{n}}_1 - \hat{\boldsymbol{n}}_2|$. The vector $\hat{\boldsymbol{e}}_2 = (\hat{\boldsymbol{p}} - (\hat{\boldsymbol{p}} \cdot \hat{\boldsymbol{e}}_3)\hat{\boldsymbol{e}}_3)/|\hat{\boldsymbol{p}} - (\hat{\boldsymbol{p}} \cdot \hat{\boldsymbol{e}}_3)\hat{\boldsymbol{e}}_3|$ is defined as the projection of the vector $\hat{\boldsymbol{p}} = \hat{\boldsymbol{r}}_1 - \hat{\boldsymbol{r}}_2$ connecting the two centers of mass, onto the plane perpendicular to $\hat{\boldsymbol{e}}_3$. The last vector is defined as $\hat{\boldsymbol{e}}_1 = \hat{\boldsymbol{e}}_2 \times \hat{\boldsymbol{e}}_3$, and it points in the direction of the symmetry axis of the DNA grooves.

The local deformations can be computed from the rotation matrix, $\mathbf{R}(n) = \mathbf{T}^T(n)\mathbf{T}(n+1)$, which generates the frame at segment $n+1$ from that at segment n. Here the 3×3 orthogonal matrix ($\mathbf{T}$), is constructed by using as columns the local reference frame vectors: $\mathbf{T}(n) = [\hat{\boldsymbol{e}}_1(n), \hat{\boldsymbol{e}}_2(n), \hat{\boldsymbol{e}}_3(n)]$ and its transpose is represented by $\mathbf{T}^T(n)$. At each position n along the rod, the components $R_{ij}(n)$ of the matrix $\mathbf{R}(n)$ are related to a rotation vector $\boldsymbol{\theta}(n) = \theta_1(n)\hat{\boldsymbol{e}}_1(n) + \theta_2(n)\hat{\boldsymbol{e}}_2(n) + \theta_3(n)\hat{\boldsymbol{e}}_3(n)$ according to the following equation:

$$\begin{pmatrix} \theta_1 \\ \theta_2 \\ \theta_3 \end{pmatrix} = \frac{\theta}{2\sin\theta} \begin{pmatrix} R_{32} - R_{23} \\ R_{13} - R_{31} \\ R_{21} - R_{12} \end{pmatrix}, \tag{S24}$$

where θ satisfies the relation: $\mathrm{trace}(\mathbf{R}) = 1 + 2\cos\theta$. Finally, the local deformations can be defined as the deviations of the components of $\boldsymbol{\theta}(n)$ from their respective mean value ($\overline{\theta_i}$) in the relaxed configuration (under no mechanical stress):

$$a\Omega_i(n) = \theta_i(n) - \overline{\theta_i}, \tag{S25}$$

where $a = 0.34$ nm is the mean distance between consecutive base-pairs. The values of $\overline{\theta_i}$ have been obtained from simulations of linear molecules in reference [4]. For oxDNA1 it was found that $\overline{\theta_1} = \overline{\theta_2} = 0$ and $\overline{\theta_3} = 34.8°$, while the same quantities for oxDNA2 are: $\overline{\theta_1} = 0$, $\overline{\theta_2} = 2.6°$ and $\overline{\theta_3} = 34.1°$. Note that in the main text we use $\chi_0 = \overline{\theta_3}/a$ as the value of Ω_3 in the relaxed sate of the DNA.

Average of the local deformations – In order to obtain the time evolution of the local deformations, we ran 100 independent configurations of the system described in section VI while we keep the temperature constant at $T = 15$ K. All the samples start with an excess/deficit of one helical turn in half of the ring and the local twist in this region is locked during equilibration. After this stage, we release the constraint on the over/under twisted region and we keep track of the local deformations over the entire ring for $1.5 \times 10^4 \tau_{LJ}$. In practice this is done by computing the average $\langle\Omega_i(n)\rangle$ over configurations of the local deformations at the same time after the twist release.

In Fig. **3** of the main text we report the values obtained for $\Omega_3(n)$ in the undertwisted case at different times. The results for the overtwisted case are shown in Fig. **4**. In both, simulations were run at 15 K. To complement this, here we show the local deformation $\Omega_3(n)$ when the temperature is fixed at $T = 300$ K (see Fig. S2). It is clear that by increasing the temperature of the system, the signal becomes noisier compared to the one depicted in Fig. **4** and the error of the diffusion coefficient computed from simulations becomes larger: $D_I^+ = 0.219 \pm 0.027$ and $D_{II}^+ = 0.168 \pm 0.022\, bp^2/\tau_{\mathrm{LJ}}$. These values are in good agreement with the ones obtained at $T = 15$ K. As pointed out in the main text, running simulations at room temperature would require to have more statistics and therefore it would be less efficient.

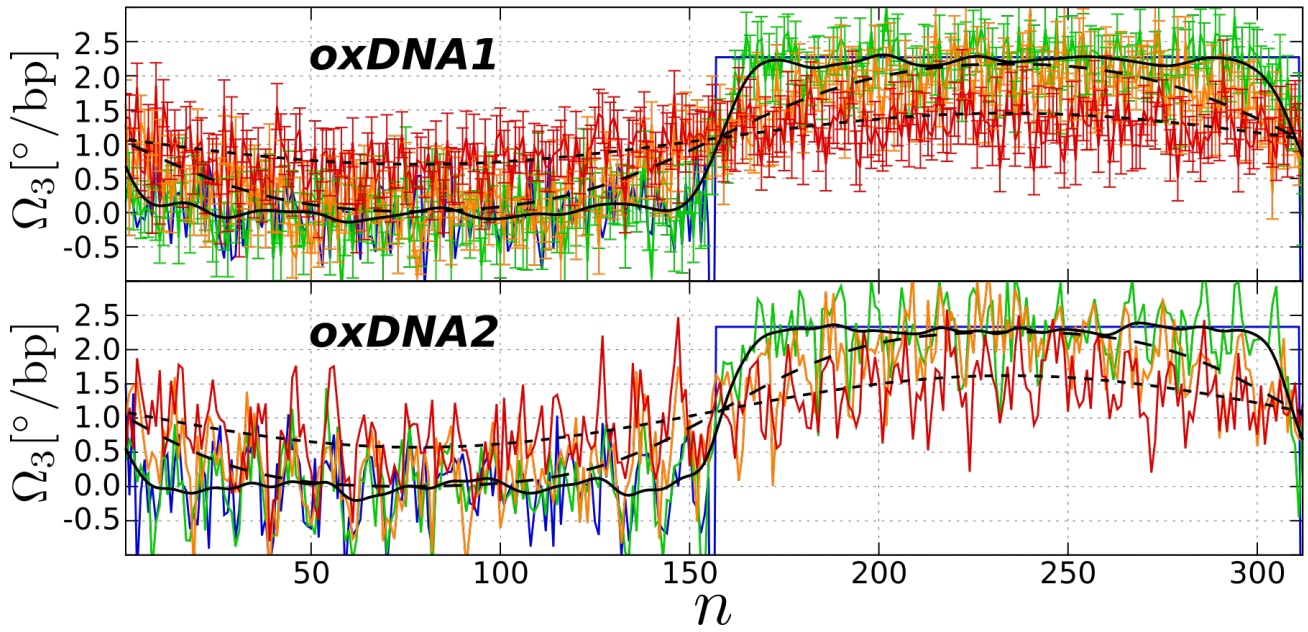

Fig. S 2 Local twist deformation (Ω_3) as function of the contour length when the temperature of the system is kept constant at $T = 300$ K. Color lines (blue, green, yellow and red) represent results at different time-steps ($t = 0, 5, 2500$ and $15000\tau_{\mathrm{LJ}}$). The diffusion coefficients found are $D_I^+ = 0.219 \pm 0.027$ and $D_{II}^+ = 0.168 \pm 0.022\, bp^2/\tau_{\mathrm{LJ}}$, in agreement with the values obtained at 15 K.

VIII Computation of the Diffusion coefficient

The diffusion equation (9) has an explicit solution that can be conveniently written in terms of the Fourier coefficients. Considering the periodic boundary conditions of our system (for ring DNA) this leads to:

$$\delta\Omega_3(t,n) = \sum_k \tilde{W}_k(t) e^{-\frac{2\pi k}{N}n} = \sum_k \tilde{W}_k e^{-\frac{4\pi^2 k^2 \tilde{D}}{N^2}t} e^{-\frac{2\pi k}{N}n} \tag{S26}$$

where $k \in \mathbb{Z}$ and the Fourier coefficients $\tilde{W}_k$ are obtained from the initial condition $\tilde{W}_k = \sum_{n=1}^{N} \delta\Omega_3(0,n) e^{\frac{2\pi k}{N}n}$. Notice that this relation holds true also in the continuum limit where $\frac{n}{N} \to s \in [0,1]$. If we focus our attention to a single modes k, we observe that comparing the Fourier coefficients at different timesteps it is possible to obtain the time-dependence:

$$\ln \frac{|\tilde{W}_k(0)|}{|\tilde{W}_k(t)|} = \tilde{D}\frac{4\pi^2 k^2}{N^2} t \tag{S27}$$

We have computed the Fourier analysis of twist for each timestep of the trajectory. Then, by using a linear fit of the Fourier coefficients via Eq. S27 (see Fig. S3), we were able to estimate the diffusion coefficient in the different models. The value we presented is a weighted average on the first 5 coefficients (the $k = 0$ mode is obviously excluded also). In our simulation, the diffusion coefficients computed on higher modes have to be excluded because the white noise combined with faster relaxation time ($\tau \propto 1/k^2$) reduce the number of data available for the exponential fit (see Fig. S3 inset). The error in the diffusion coefficient is obtained from the standard error-propagation formula applied to the errors resulting from the previous fit.

In the oxDNA2 model ($G > 0$) there is a further observation to do: the twist Ω_3 shows waves due to the coupling with Ω_2 (see Fig. **4**(**D**)). These waves have a characteristic frequency equal to the pitch of DNA, one turn every 10.5 base pairs. If we reconstruct this signal using only the low frequencies of the Fourier Transform of Ω_3, we get a curve that passes through the centerline of the wave. From the fit of the diffusion equation to the data we obtain a curve that follows basically the same trajectory. The same behavior is found for Ω_2 in agreement with our theory (see also Fig. **4**).

IX Evolution of the total Twist

At any fixed timestep from the simulation, the total twist (Tw) is found from adding the value of the local twist θ_3 along all the base-pairs:

$$\mathrm{Tw} = \frac{1}{2\pi}\sum_{n=1}^{N} \theta_3(n). \tag{S28}$$

Therefore, the sum of the twist deformations is related to the deviations of the total twist from its value under no torsional stress (Tw_0) according to:

$$\mathrm{Tw} - \mathrm{Tw}_0 = \frac{1}{2\pi}\sum_{n=1}^{N} a\Omega_3(n). \tag{S29}$$

When the ring molecule is constraint by the two parallel planes, the initial writhe is preserved during the whole simulation ($\mathrm{Wr}(t) = 0$) and Eq. (S29) gives a constant value of, for example, -1 for molecules initialized in the undertwisted case. On the other hand, when we remove the planes from the simulations the value of Wr changes with time. There is an exchange of twist and writhe that obeys the White-Fuller-Calugarenau the-

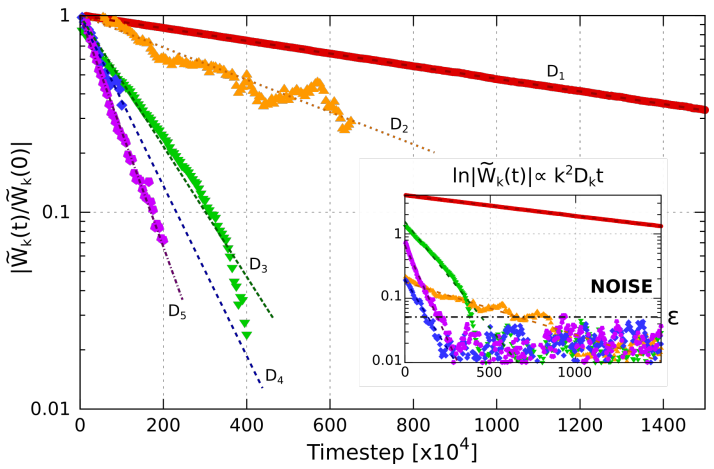

Fig. S3 Calculation of the Diffusion coefficient from the Fourier Analysis. Equation S27 predicts for the Fourier modes of the twist local deformation an exponential decay with time. In the main plot, time evolution of the first modes, $k=1$ red, $k=2$ yellow, $k=3$ green, $k=4$ blue, $k=5$ purple, are shown with respect to their initial values and the dashed lines represent the exponential fit. Since the noise set a limit below which no information could be extracted, the exponential are fitted in the range $t\in[0,T_\epsilon]$ where T_ϵ is the largest values for which $|\tilde{W}|_k(t)>\epsilon\,\forall\, t<T_\epsilon$. Data from all the coefficients and the level of noise ϵ are shown in the inset. Using the fit parameters it is possible to estimate the values of the diffusion constant $D_k=a_k\frac{N^2}{4\pi^2k^2}$.

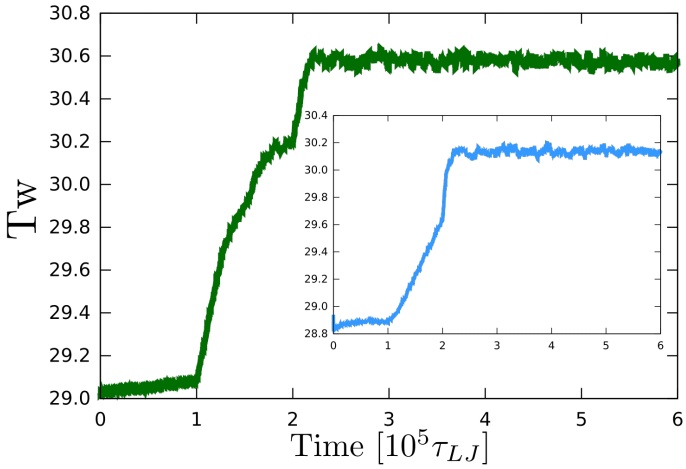

Fig. S 4 Time evolution of the total twist for oxDNA1 (green) and oxDNA2 (cyan). Results are obtained from simulations at $T=15$ K.

orem: $\mathrm{Lk}=\mathrm{Tw}(t)+\mathrm{Wr}(t)$, where Lk is constant.

The writhing of the molecule requires global conformational changes and hence is a slow process compared to the diffusion of the local twist. Therefore, to be able to track the writhe evolution (or analogously $\mathrm{Tw}(t)$) we had to speed up our simulations. The standard way of doing this in molecular dynamics simulations (see section VI), is to use a high diffusion constant, which in turn means to use a high inertial time τ_{in}.

We ran simulations for a total time of $(6\times10^5\tau_{\mathrm{LJ}})$. Initially, the inertial time was set to $\tau_{in}=0.03\tau_{\mathrm{LJ}}$. After $1\times10^5\tau_{\mathrm{LJ}}$ we increased its value to $\tau_{in}=1\tau_{\mathrm{LJ}}$. A second increased to $\tau_{in}=10\tau_{\mathrm{LJ}}$ was applied at time-step $2\times10^5\tau_{\mathrm{LJ}}$. The results of the total twist following this protocol and average over three independent configurations are shown in Fig. S4 for undertwisted ring DNA molecules when the temperature is set to 15 K. In Fig. **5** of the main text we report the same results after rescaling the units of time by a factor of $1/0.03=33.33$ during the first increment in τ_{in} and by a factor ten times larger during the second increment.

X Bending modes

As explained in the main text, the dynamics of twist can be divided in two stages. At times $t<t^*$ the deficit of local twist diffuses across the entire ring, keeping the total twist constant in the process. In other words, there is no production of writhe. At $t>t^*$ the buckling of the molecule might begin. The analysis for the isotropic TWLC model indicates that there is a critical value of the linking number excess $\Delta\mathrm{Lk}=\mathrm{Lk}-\mathrm{Lk}_0$, beyond which the planar configuration becomes unstable and the ring buckles and folds on itself[9]. According to the linear stability analysis, a characteristic frequency ϕ_m for the initial out of plane deformations with mode number m is determined by the following equation

$$\phi_m^2=\frac{A}{\rho_0R_0^4}\left(f_m-\frac{2\pi C\Delta\mathrm{Lk}}{A}g_m\right), \tag{S30}$$

where $\rho_0=3.3\times10^{-15}kg/m$, R_0 is the radius of the ring with constant curvature, $f_m=m^4+3m^2+1/2$ and $g_m\approx m^3/2$. The most unstable mode (m^*) corresponds to the minimum of the ϕ_m^2 and it can be found as the solution to:

$$4m^3-\frac{3\pi C\Delta\mathrm{Lk}}{A}m^2+6m=0. \tag{S31}$$

Therefore, the theory does not predict any dependence of m^* on the total length of the molecule but only on the ratio $\frac{C}{A}$ and ΔLk. We expect that this mode will grow faster than the others, and thus will be the first observed at the onset of the buckling.

We now compare the prediction of the isotropic TWLC model (Eq. (S30)) with our numerical observations. By doing so, recall that the number of elastic parameters for our numerical models is larger than two. We therefore attempt to map the elastic behaviors of oxDNAs to that of an isotropic TWLC using their rescaled elastic constant $\tilde{A}$ and $\tilde{C}$. Results are displayed in Fig. S5, where we plot ϕ_m^2 for $\Delta\mathrm{Lk}=0,1,2$ (analogous results are expected for negative values of ΔLk, see[9]) using the ratio $\tilde{C}/\tilde{A}$ of oxDNA1 (2.04) and oxDNA2 (1.6). From our line of reasoning, one expects that the smaller the ratio $\tilde{C}/\tilde{A}$, the smaller the selected mode number m^* at a fixed ΔLk. We find that, while for oxDNA1 the minimum of ϕ_m^2 is located at $m^*\simeq4$, for oxDNA2 it is smaller $m^*\simeq3$. We also note that according to the linear stability analysis (Eq. (S30)) the value of ΔLk at which ϕ_m^2 becomes negative (indicating the ring instability) depends on the elastic constants of the system: the smaller the (C/A) ratio the larger the critical $|\Delta\mathrm{Lk}|$ required to initiate the buckling transition. For the oxDNA models this transition happens at $|\Delta\mathrm{Lk}|\geq1$.

Since the writhing of the molecule is reflected in Ω_1 and Ω_2 for both the oxDNA models, we can track the bending modes (m) by looking at, for example, the number of minima (or maxima) that the envelope of Ω_2 has at a certain time. This number is shown

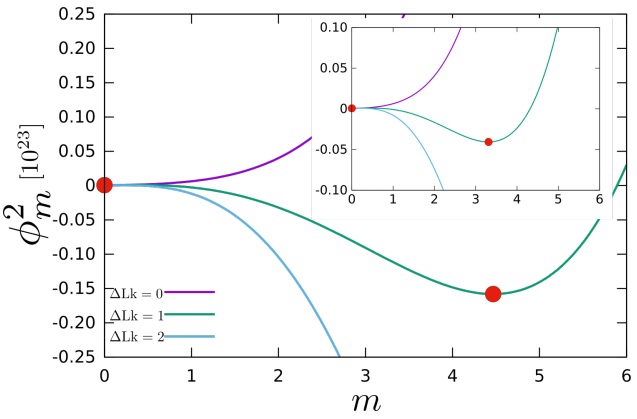

Fig. S5 Reduced frequencies from Eq. (S30) against the mode number m, for different levels of supercoiling. At $\Delta\mathrm{Lk} = 1$ the value of ϕ_m^2 becomes negative, indicating the instability of the circle. The main figure shows results for the oxDNA1 model and the inset for oxDNA2. Minimum of each curve is depicted with a red dot.

at the bottom of supplementary movies S1-S2 and depicted as a function of time in Fig. S6. We observe that several modes start emerging on time until one particular mode is selected: $m^* = 4$ for oxDNA1 and $m^* = 3$ for oxDNA2 as predicted by Eq. (S31) (see also Fig. S5). However, it is worth mentioning here that this behavior is only true at early times. We expect that if we wait long enough until equilibration, the molecule will show the usual eight-shape (for a ring initialized with $|\Delta\mathrm{Lk}| = 1$) and therefore the number of modes at long times will be in general smaller than m^*.

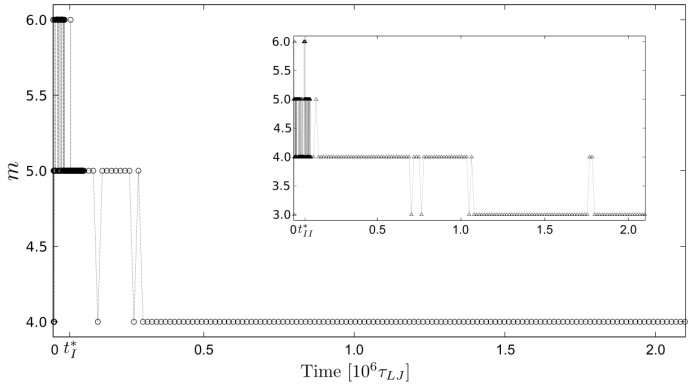

Fig. S6 Time evolution of the bending mode number for a molecule 312 bp long simulated with the oxDNA1 and oxDNA2 (inset) models. Lines are a guide for the eye. Here we also observe that the selected mode numbers at the onset of buckling are $m^* = 4$ (oxDNA1) and $m^* = 3$ (oxDNA2). See also Supplementary movies.

Since equations (S30) and (S31) were obtained for an isotropic TWLC without twist-bend coupling, there are some features in our simulations that the theory is not able to capture. We found for example that for the oxDNA models there is always an initial increase of the selected bending mode with the ring size. This is shown in Fig. **6** for rings with $L = 312, 624$ and 936 bps and two values of linking deficit $\Delta\mathrm{Lk} = -1, -2$.

As discussed in the main text, when $G = 0$, the amplitude of the oscillations in the bending deformations (Ω_1 and Ω_2) decreases with the size of the ring. This implies that the anisotropic case should tend to the isotropic case as L becomes much larger than the persistence length. Therefore, at $L \gg l_b$ we should recover the no-dependence of the selected mode m^* on the ring size. We believe that is the reason why the results for oxDNA1 with $\Delta\mathrm{Lk} = -1$ show a plateau in Fig. **6** of the main text. We also expect that when $L \sim l_b$ in the anisotropic case, the larger the linking deficit the less modes observed for undertwisted rings. The net effect would be then the slow down of the growth of m^* with L. Therefore, we expect that the plateau of m^* would be reached at larger lengths as we increase the linking deficit. This is consistent with the results for oxDNA1 with $\Delta\mathrm{Lk} = -2$ in Fig. **6** of the main text. The exact dependence of m^* on L and $\Delta\mathrm{Lk}$ is beyond the scope of this manuscript.

XI Movies

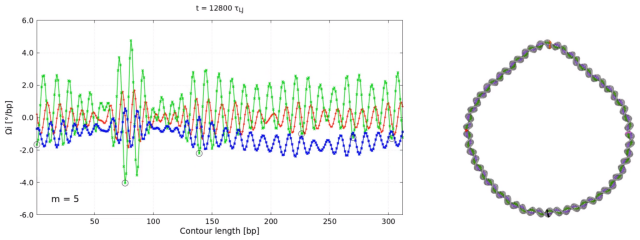

Movie S1 Time evolution of the local deformations for the system simulated with the oxDNA2 model after removing the planes and releasing the twist. **Left** panel shows Ω_1 (red), Ω_2 (green) and Ω_3 (blue) at the time indicated at the top of the image. The twist-bend coupling induces the twist waves. Ω_2 and Ω_3 are in antiphase as described in Eq. 4. The local minima of the Ω_2 envelope are depicted by black circles. Therefore, the number of black circles (considering the periodicity of the system) at a fixed time, is the number (m) of bending modes of the system. This is shown at the bottom of the image. **Right** panel shows the configuration of the system corresponding to the left plot. Four base-pairs located at position $n = 1, 78, 156$ and 234 of the contour length are indicated with colors: pink, orange, red and black.

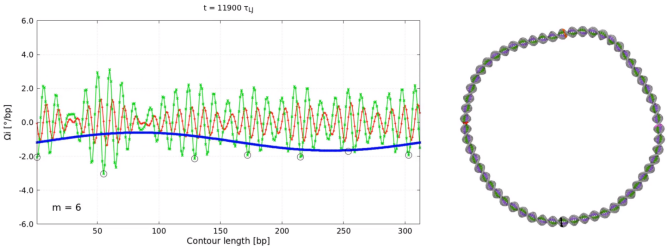

Movie S2 Time evolution of the local deformations for the system simulated with the oxDNA1 model after removing the planes and releasing the twist. **Left** panel shows Ω_1 (red), Ω_2 (green) and Ω_3 (blue) at the time indicated at the top of the image. The local minima of the Ω_2 envelope are depicted by black circles. Therefore, the number of black circles (considering the periodicity of the system) at a fixed time, is the number (m) of bending modes of the system. This is shown at the bottom of the image. **Right** panel shows the configuration of the system corresponding to the left plot. Four base-pairs located at position $n = 1, 78, 156$ and 234 of the contour length are indicated with colors: pink, orange, red and black.

References

1 M. Caraglio, E. Skoruppa and E. Carlon, *The Journal of Chemical Physics*, 2019, **150**, 135101.

2 E. Skoruppa, S. K. Nomidis, J. F. Marko and E. Carlon, *Phys. Rev. Lett.*, 2018, **121**, 088101.

3 F. B. Fuller, *Proceedings of the National Academy of Sciences*, 1978, **75**, 3557–3561.

4 E. Skoruppa, M. Laleman, S. K. Nomidis and E. Carlon, *The Journal of Chemical Physics*, 2017, **146**, 214902.

5 O. Henrich, Y. A. G. Fosado, T. Curk and T. E. Ouldridge, *Eur. Phys. J. E*, 2018, **41**, 57.

6 S. Plimpton, *J. Comp. Phys.*, 1995, **117**, 1–19.

7 T. Ouldridge, *PhD thesis*, University of Oxford, 2011, 2011.

8 J. P. K. Doye, T. E. Ouldridge, A. A. Louis, F. Romano, P. Šulc, C. Matek, B. E. K. Snodin, L. Rovigatti, J. S. Schreck, R. M. Harrison and W. P. J. Smith, *Phys. Chem. Chem. Phys.*, 2013, **15**, 20395–20414.

9 F. Tanaka and H. Takahashi, *The Journal of Chemical Physics*, 1985, **83**, 6017–6026.